Università degli Studi Mediterranea di Reggio Calabria
Archivio Istituzionale dei prodotti della ricerca

Artificial Lossy Backgrounds to Improve Linear Electromagnetic Imaging Inside PEC Enclosures

This is the peer reviewd version of the followng article:

Original
Artificial Lossy Backgrounds to Improve Linear Electromagnetic Imaging Inside PEC Enclosures / Cheraghi, A; Bevacqua, M; Jeffrey, I; Gilmore, C. - In: IEEE ANTENNAS AND WIRELESS PROPAGATION LETTERS. - ISSN 1536-1225. - 22:4(2023), pp. 724-728. [10.1109/LAWP.2022.3223299]

Availability:
This version is available at: https://hdl.handle.net/20.500.12318/136027 since: 2024-09-14T14:05:22Z

Published
DOI: http://doi.org/10.1109/LAWP.2022.3223299
The final published version is available online at:https://ieeexplore.ieee.org/document/9954610

Terms of use:
The terms and conditions for the reuse of this version of the manuscript are specified in the publishing policy. For all terms of use and more information see the publisher's website

Publisher copyright

This item was downloaded from IRIS Università Mediterranea di Reggio Calabria (https://iris.unirc.it/) When citing, please refer to the published version.

(Article begins on next page)

13 January 2025

Artificial Lossy Backgrounds to Improve Linear Electromagnetic Imaging inside of PEC Enclosures

Amirreza Cheraghi, *Student Member, IEEE*, Martina T Bevacqua *Member, IEEE*, Ian Jeffrey *Member, IEEE*, and Colin Gilmore, *Senior Member, IEEE*

***Abstract*—Herein we propose the use of artificial (or numerical) backgrounds for electromagnetic inversion inside of conducting enclosures. Such enclosed imaging systems are used both due to external constraints (e.g, grain bin imaging), or in order to provide external shielding and easy-to-model boundary conditions (e.g., in stroke or breast imaging systems). We use the Orthogonality Sampling Method (OSM), although the use of such artificial backgrounds is independent of the imaging method. Using a set of 2D simulated examples, we show that the performance of OSM is generally poor inside of such PEC enclosures if the background material surrounding the target is lossless. However, we show that performance of OSM can be greatly improved through the use of artificial lossy backgrounds. With such artificial backgrounds, the imaging experiment can take place in a lossless PEC enclosure, but one can compute the scattered fields relative to an arbitrary lossy background, then perform OSM inside of that artificial lossy enclosure. The introduction of loss in the background problem can improve the performance of OSM when the average target permittivity is approximately known.**

***Index Terms*—Orthogonal Sampling Method, Back propagation, Inversion**

I. Introduction

ELECTROMAGNETIC inversion is the process of illuminating a target with electromagnetic waves and from the field measurements attempting to reconstruct the target. In most cases, the inversion problem is treated with a radiating boundary condition. However, we have been working in the context of Grain-bin Electromagnetic Imaging (EMI) system (e.g. [1], [2]), where the electromagnetic boundary is metallic (as physical grain storage bins are almost all made of steel) and we thus have no choice but to work within enclosed imaging systems. Other electromagnetic inversion systems include semi-resonant biomedical imaging systems with large areas of metallic boundaries [3], [4], where the advantages of enclosed systems include the ability to shield outside cabling and easily model the boundary conditions. Several others have considered such enclosed imaging systems both theoretically and experimentally [5]–[8].

It is within the context of metallic-enclosed boundaries that we are interested in non-linear imaging problems. However, we seek prior information for these non-linear problems through linear algorithms: in particular we consider herein the Orthogonality Sampling Method (OSM) [9], [10]. OSM is advantageous in that it can be re-formulated for arbitrary backgrounds and near-field systems [11], [12]. In this paper we consider the use of OSM for the discrimination of the air-grain interface [13], [14] inside metallic enclosures. Similar to other researchers who considered a large number of non-linear reconstructions inside of a PEC enclosure [5] within a lossless background (e.g. relative permittivity $\epsilon_r = 1$), we have found that OSM and other back propagation methods have very poor performance for a wide range of frequencies. The reason for this poor performance is not fully understood, but it has been noted that the poor performance occurs around the resonances of the chamber [5], and that inside of circular chambers with a radius greater 1 wavelength, almost all lossless reconstructions are poor (there are many resonances that are difficult to avoid).

To alleviate the fact that imaging techniques usually break down when formulated with lossless backgrounds in PEC chambers, the main contribution of this work is to introduce the concept of an artificial lossy background. 'Artificial' in the sense that even though the main imaging experiment is performed in a lossless background, we can significantly improve the imaging results by calculating the scattered fields with respect to an arbitrary lossy background, then performing the inversion with respect to that artificial lossy background. This is similar to the 'numerical' backgrounds proposed in [15], but our focus is on improving results inside of resonant enclosures, which tend to perform poorly in the lossless case. The important point is that this artificial lossy background need not be part of the physical experiment: it is a purely artificial construct used as part of the inversion algorithm (many others have already considered lossy backgrounds, e.g., [3], [5], but as part of both experiment and inversion).

To test our idea of such backgrounds, we use OSM as an inversion method. The implications of the enclosed system performance break down and the ability to improve the results through artificial backgrounds go beyond OSM. In particular, the Contrast Source Inversion method usually uses back-propagation as its initial guess, thus these observations will affect CSI-based inversion in enclosed systems as well [16].

This work is an extension to that in [14], where we used back-propagation and showed (in a single example) the possibility that the use of an artificial lossy background could improve the final image. In this work, we extend those preliminary results by showing how this process fits into OSM, show the limitations of our approach through a larger set of examples, and provide an arguments as to why artificial lossy backgrounds can improve imaging results.

AC,IJ, and CG are with Dept. of Electrical and Computer Engineering, University of Manitoba, Winnipeg, Canada. MB is with Università Mediterranea, Reggio Calabria, Italy.

Manuscript received June 2022;

This is the post reviewed version of the following article: A. Cheraghi, M. T. Bevacqua, I. Jeffrey and C. Gilmore, "Artificial Lossy Backgrounds to Improve Linear Electromagnetic Imaging Inside PEC Enclosures," in IEEE Antennas and Wireless Propagation Letters, vol. 22, no. 4, pp. 724-728, April 2023, doi: 10.1109/LAWP.2022.3223299. Article has been published in final form at: https://ieeexplore.ieee.org/document/9954610.

II. Overview of OSM Method and Its use In Enclosed Systems

OSM is a qualitative linear imaging method that can be used to retrieve the support of unknown imaging targets. It can be implemented for multi-view multi-static, single-view, multi-frequency, or a combination of these [17]. OSM is capable of imaging heterogeneous objects and objects with discontinuities [17]. Herein, we assume the 2D scalar Helmholtz equation. OSM creates an image of the target through the use of a 'reduced scattered field', which are directly related to the radiating components of the currents induced in the object by the incident field [17]. The reduced scattered fields are defined as:

$$u^{sct}_{red}(\mathbf{r}', \mathbf{r_t}) = \left\langle u^{sct}(\mathbf{r}, \mathbf{r_t}), G_{bkg}(\mathbf{r}; \mathbf{r}') \right\rangle_{\Gamma}, \tag{1}$$

where u^{sct} denotes the (measured) scattered field, G_{bkg} denotes the Green's function pertaining to the background medium surrounding the target. Γ indicates the measurement surface, $\mathbf{r}$ is the receiver positions, $\mathbf{r_t}$ indicates the transmitter position, and $\mathbf{r}'$ is a variable that moves over the support of the target (i.e. the imaging domain).

Assuming that we have a continuous set of receiver points, Eq. (1) can also be written as [17], [18]:

$$u^{sct}_{red}(\mathbf{r}', \mathbf{r_t}) = \int_{\Gamma} G_{bkg}(\mathbf{r}; \mathbf{r}')^H \; u^{sct}(\mathbf{r}, \mathbf{r_t}) \, d\mathbf{r}. \tag{2}$$

In practice, we have a discrete set of receiver points and the integral over the domain Γ becomes a finite sum over each receiver point. The reduced scattered field $u^{sct}_{red}(\mathbf{r}', \mathbf{r_t})$ can be calculated for each location $\mathbf{r}'$ inside the imaging domain, for each transmitter.

To create an image out of this information, OSM introduces the indicator function which is the L2-norm of the reduced scattered field: [17].

$$I(\mathbf{r}') = \int_{\Gamma^t} |u^{sct}_{red}(\mathbf{r}', \mathbf{r_t})|^2 \, d\mathbf{r_t} = \left\| u^{sct}_{red}(\mathbf{r}', \mathbf{r_t}) \right\|^2_{\Gamma^t} \tag{3}$$

where Γ^t indicates the transmitter surface. In practice, where we have discrete transmitters, the integral above becomes a sum over transmitters. The indicator function has large values where the induced currents are high (typically inside the scatterer), and lower values for the regions where no scattering currents exist (typically outside the scatterer). For multi-frequency cases, one can simply integrate indicator functions over each frequency [17].

To implement OSM inside of enclosures, in this paper we simply use the Green's function associated with that enclosure. Details on implementation are in section III.

A. The use of Artificial Backgrounds in OSM

Consider the total fields that are collected as part of the actual lossless physical experiment: outside of the imaging target (which may be lossless or lossy) a lossless medium is present within the metallic enclosure, see, e.g., Fig 1. Denote these fields as u^{tot}. These fields are due to the boundary, sources, and presence of the target in a losselss background. Next, define an artificial incident field problem by assuming a known permittivity distribution everywhere in the enclosure. The known distribution is referred to as the artificial background medium, which for simplicity we assume is homogeneous herein (but in general may be inhomogeneous). Within the inverse scattering problem, we are free to specify an artificial background, and that in turn defines the incident fields, which we refer to as u^{inc}_{lossy}. These incident fields satisfy the same set of sources and boundary conditions.

These two fields satisfy the equations

$$\nabla^2 u^{tot}(\mathbf{r}) + k^2_{tot}(\mathbf{r}) u^{tot}(\mathbf{r}) = -s(\mathbf{r}) \quad + \text{BCs} \tag{4}$$

$$\nabla^2 u^{inc}_{lossy}(\mathbf{r}) + k^2_{inc} u^{inc}_{lossy}(\mathbf{r}) = -s(\mathbf{r}) \quad + \text{BCs} \tag{5}$$

where BCs are boundary conditions, and $k = \omega^2 \sqrt{\mu\epsilon(\mathbf{r})}$ is the wavenumber and $s(\mathbf{r})$ are the sources. By defining the scattered fields in this case as:

$$u^{sct}_{lossy} = u^{tot} - u^{inc}_{lossy} \tag{6}$$

we can then subtract (5) from (4), perform some algebra, and get:

$$\nabla^2 u^{sct}_{lossy}(\mathbf{r}) + k^2_{inc} u^{sct}_{lossy}(\mathbf{r}) = -\left(k^2_{tot}(\mathbf{r}) - k^2_{inc}\right) u^{tot}(\mathbf{r}). \tag{7}$$

With (7) we can then define an inverse problem in the scattered field with contrast sources of $\left(k^2_{tot}(\mathbf{r}) - k^2_{inc}\right) u^{tot}(\mathbf{r})$.

Considering this, our artificial background workflow is:

1) Generate the synthetic total field data, $u^{tot}_{lossless}$ for the target in a lossless background ($\epsilon_r = 1$) with a PEC boundary.
2) Generate the background Green's function matrix G_{bkg} for an artificially selected, but lossy permittivity background, with the same PEC boundary. The background permittivity does not need to match any permittivity used in the target data set. In the case of a physical experiment, this step is not required.
3) Calculate the scattered fields from Eq. (6).
4) Calculate OSM indicator function (i.e Eq (3)) with respect to this 'artificial' background medium by processing the data in step 3.

III. Results

Within this work, we use a Discontinuous Galerkin Method (DGM) forward solver [19], [20] to generate the matrix G_{bkg}. Using the adjoint approach, we place a point source at the receiver location, then calculate the resultant fields within the imaging region. Each call of this forward solver then generates a row of the matrix G_{bkg}. Using this method, the analytical version of the Green's function does not need to be calculated, and any arbitrary PEC or radiating boundary with near field or far field receiver positions is supported.

A. Austria Target

As our first example, we have used a version of the 'Austria' target shown in Fig. 1, embedded in a circular boundary. The mesh was generated using GMSH [21]. The object consists of a larger circle with radius of 0.6 m, and two small disks with radii of 0.2 m. The boundary of imaging enclosure is a circle centered at the origin with radius of 1.5 m. There are 36 antennas acting as either transmitter or receiver that

have been placed uniformly on the circumference of an origin-centered circle with radius of 1.4 m. We have chosen to place the transceiver points 10 cm away from the PEC as this matches the approximate location of the antennas in a grain-bin imaging system [1].

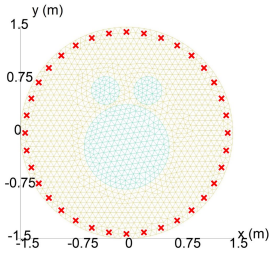

Fig. 1. 'Austria' imaging experiment setup, inside a circular boundary with radius of 1.5 m and 36 transceivers distributed uniformly inside the boundary, on a circle with radius of 1.4 m.

The entire target has the relative dielectric permittivity of $\epsilon_r = 2 - j0.6$, and other regions in the mesh are lossless vacuum ($\epsilon_r = 1$). The frequency range used in the simulation is between 200 MHz to 250 MHz with 10 MHz steps (mid-frequency the enclosure radius is 0.89λ). For each frequency, all the transmit/receive pairs have been simulated, but not the self interaction (36×35). Also, for obtaining the numerical Green's function, a 2 m $\times$ 2 m square (large enough to surround the entire target) has been discretized into a 40×40 grid, assuming pulse basis functions. The incident, total, and scattered fields were simulated from this target for both a radiating and PEC boundary conditions.

To provide a baseline of OSM performance, we first present the multi-frequency OSM results on this target with radiating boundary conditions. These results are shown in Fig. 2 (left) and show that at these frequencies, the target is reconstructed well. Next, we applied OSM to the fields generated with the PEC boundary. In this case, both the fields and the background Green's function matrix G_{bkg} are generated with the PEC boundary, with a lossless background. These results are shown in Fig. 2 (right). This result shows how OSM does not perform well inside of a lossless PEC background (despite the use of a large number of frequencies and transmit/receive pairs). The results match the observations of other researchers [5].

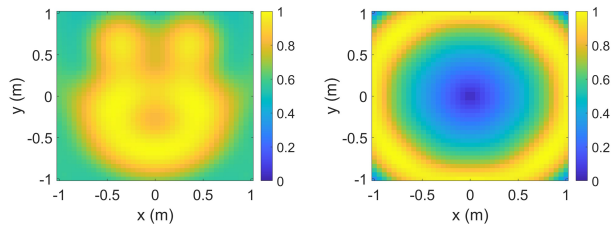

Fig. 2. Left: Normalized OSM reconstruction when the background is lossless vacuum and the boundary is a radiating boundary condition. Right: Normalized OSM Reconstruction when the the background is lossless and the boundary condition is a PEC.

B. Artificial backgrounds to improve PEC enclosed OSM

For a first example of our proposed artificial background process, we repeated the experiment but following our artificial background workflow. For the result in Fig. 3 (left) we used an artificial background for OSM of $\epsilon_{bkg} = 2 - j0.6$ (i.e., we matched the target permittivity). In this case, the overall shape of the target is clear. We note that the use of this background means that the air regions become high-contrast and then correspond to indicator value close to 1, while the target ideally corresponds to indicator function values of 0.

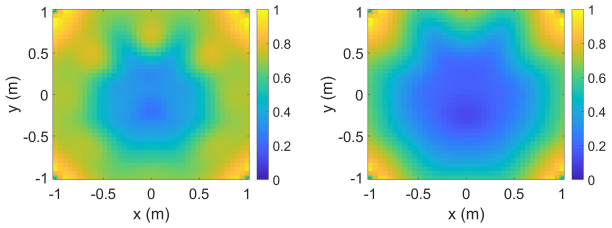

Fig. 3. Normalized OSM Reconstruction when the experiment is in a lossless background, but artificial lossy backgrounds are used in reconstruction. Left: Lossy background of $\epsilon = 2 - j0.6$, Right: Lossy background of $\epsilon = 1 - j0.6$. Note, as the backgrounds are not free space, the indicator function is lower inside the target.

Next, we consider the use of an artificial background that does not match the permittivity of the target. In this example, the artificial background is selected to be the Green's function associated with the permittivity $\epsilon_{bkg} = 1 - j0.6$. These results are shown in Fig. 3 (right). While the target has become more blurred (see, e.g., the far left and right-hand sides of the image), the overall shape of the target is still visible.

C. Artificial Backgrounds In a 2D Model Grain Bin

Next we consider synthetic example of a 2D grain bin model (see Fig. 4). The model is 10 m across with a trapezoidal roof and 24 transceivers have been distributed uniformly on the two walls and floor of the bin 10 cm away from the PEC boundary. We select frequencies from 40 MHz to 80 MHz in 10 MHz frequency steps. The assumed grain position is shown in Fig. 4 top-left. The grain relative permittivity was set to $3 - j0.5$ for all frequencies. One of the challenges in this example is the fact that antennas are located inside the boundary of the problem and the object under test, which is unavoidable in grain bin imaging. For these images, we are showing an indicator function wherein the reduced scattered fields are solved for the back-propagated contrast (and are weighted by the incident field as done in eq. (38) in [22]). This approach assumes the Born approximation and solves for the contrast (see [13] for details) and this approach can improve the results [13].

It is clear from these results that in the lossless reconstruction the grain surface is not visible. If we switch the artificial background to $\epsilon_{bkg} = 3 - j0.5$, the grain surface becomes visible. The final result shows the contrast with a artificial lossy background of ($\epsilon_{bkg} = 2.8 - j0.4$) and this change shows the imaging method can work when there is some error in the assumed permittivity.

To further expand on how accurate ϵ_{bkg} needs to be, in Fig. 5 we have further considered $\epsilon_{bkg} = 1 - j0.5$, $\epsilon_{bkg} = 3 - j0.1$, $\epsilon_{bkg} = 3 - j0.9$, and $\epsilon_{bkg} = 5 - j0.5$. In both the low-loss case ($\epsilon_{bkg} = 3 - j0.1$) and the case with the largest difference between the target and background ($\epsilon_{bkg} = 5 - j0.5$), the grain surface is not visible. These results indicate that it is best to have some loss in the background while minimizing the contrast with the target (i.e., it is preferable that ϵ_{bkg} be as close as possible to the value of the target).

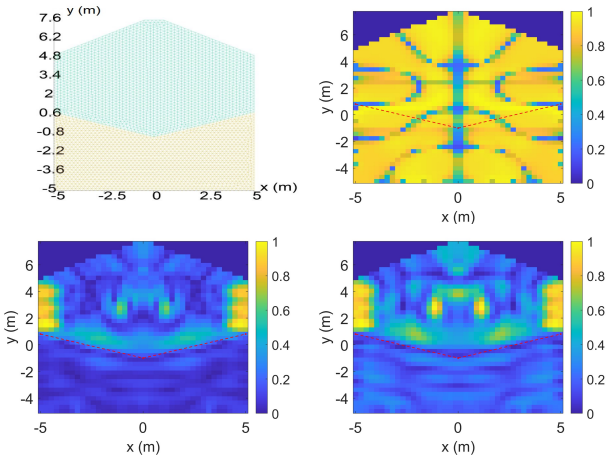

Fig. 4. Top-left: A 2D synthetic model of a grain bin, including grain (yellow) and air (green). Top-right: Normalized reconstruction of back-propagated contrast inside a lossless background medium. Bottom-left: Normalized reconstruction of back-propagated contrast inside a lossy background of $\epsilon_{bkg} = 3 - j0.5$. Bottom-right: Normalized reconstruction of back-propagated contrast inside a lossy background of $\epsilon_{bkg} = 2.8 - j0.4$.

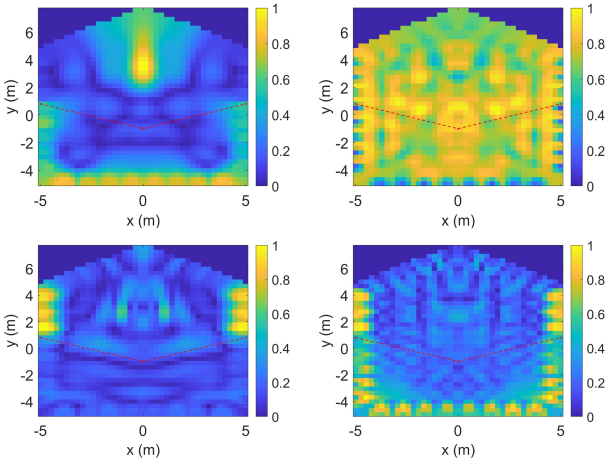

Fig. 5. Further back-propagated reconstructions of the grain bin with various ϵ_{bkg}. Top-left: $\epsilon_{bkg} = 1 - j0.5$, Top-right: $\epsilon_{bkg} = 3 - j0.1$, Bottom-left: $\epsilon_{bkg} = 3 - j0.9$, Bottom-right: $\epsilon_{bkg} = 5 - j0.5$.

IV. Discussion

While we have no satisfying mathematical explanation why imaging fails in the lossless PEC case, some qualitative arguments can be provided. As discussed in [5], the fields inside the enclosure consist of a complex set of standing waves with many resonances, and at the resonant frequencies the lossless Green's function has a division by zero in many locations in the enclosure.

Further, near these resonances, the singular value spectrum of the (incident) Green's function operator G^H_{bkg} becomes dominated by a single singular value and the associated resonant mode [6]. In practice, this means the amount of recoverable information about the target is limited, as the number of singular values in the operator relates to the information that can be recovered [6]. When imaging at an incident field resonance, the incident Green's function acts as a filter that only allows information about a single resonant mode to affect the scattered fields. Thus, the only information available in the scattered fields about the contrast sources is information about that particular mode. For example in a rectangular enclosure, that mode would be a set of sine functions. Any imaging method would thus have to attempt to reconstruct a complex set of contrast sources via this single spatial frequency. Changing the incident Green's function to a lossy background eliminates this problem: the singular value spectrum of the G^H_{bkg} operator with a lossy background contains many modes (and thus many different singular values). While we could possibly image successfully in a lossless background by avoiding the resonances as in [5], inside of non-standard enclosures like the grain bin we cannot analytically compute the frequencies where these resonances occur. However, by changing to an artificial lossy background, we avoid the dominance of a single spectral mode in the G^H_{bkg} operator, thus improving the amount of recoverable information. It is possible to change the placement of the antennas to avoid this single mode dominance inside of a circular PEC (which can also be viewed as placing the antennas so that a 'meaningful' incident field reaches the target). We have not considered this placement of antennas as our positions match experimental systems [1], [3], and the experimental advantages of enclosed imaging systems require that antennas be placed close to the wall (thus hiding cabling, etc.).

V. Conclusion

In this letter, we have introduced two major points: (1) we have seen that OSM does not work well inside of lossless PEC-enclosed imaging systems; and (2) through the use of artificial backgrounds - where one can calculate the reduced scattered field for an artificial background not part of the actual experiment - one can improve the results inside of such enclosures when the average target permittivity can be estimated. . The reasons for the failure of linear imaging methods such as OSM inside PEC boundaries in a lossless background medium are not well known at this point; nevertheless, these imaging failures can be mitigated by artificially adding loss to the background in the reconstruction. Importantly, this loss does not need to be added to the actual imaging experiment. Future work will investigate the boundaries of how incorrect the permittivity can be, as well as to analyze the eigenvalues or singular values of the artificial Green's function.

REFERENCES

[1] J. LoVetri, M. Asefi, C. Gilmore, and I. Jeffrey, "Innovations in electromagnetic imaging technology: The stored-grain-monitoring case," *IEEE Antennas and Propagation Magazine*, vol. 62, no. 5, pp. 33–42, 2020.

[2] C. Gilmore, I. Jeffrey, M. Asefi, N. T. Geddert, K. G. Brown, and J. Lovetri, "Phaseless parametric inversion for system calibration and obtaining prior information," *IEEE Access*, vol. 7, pp. 128 735–128 745, 2019.

[3] M. Asefi, A. Baran, and J. LoVetri, "An experimental phantom study for air-based quasi-resonant microwave breast imaging," *IEEE Transactions on Microwave Theory and Techniques*, vol. 67, no. 9, pp. 3946–3954, 2019.

[4] J. Winges, L. Cerullo, T. Rylander, T. McKelvey, and M. Viberg, "Compressed sensing for the detection and positioning of dielectric objects inside metal enclosures by means of microwave measurements," *IEEE Transactions on Microwave Theory and Techniques*, vol. 66, no. 1, pp. 462–476, 2017.

[5] A. Fedeli, M. Pastorino, A. Randazzo, and G. L. Gragnani, "Analysis of a nonlinear technique for microwave imaging of targets inside conducting cylinders," *Electronics*, vol. 10, no. 5, p. 594, 2021.

[6] L. Crocco and A. Litman, "On embedded microwave imaging systems: retrievable information and design guidelines," *Inverse Problems*, vol. 25, no. 6, p. 065001, 2009.

[7] C. Gilmore and J. LoVetri, "Enhancement of microwave tomography through the use of electrically conducting enclosures," *Inverse Problems*, vol. 24, no. 3, p. 035008, 2008.

[8] ——, "Corrections to the 'enhancement of microwave tomography through the use electrically conducting enclosures'," *Inverse Problems*, vol. 26, no. 1, p. 019801, 2009.

[9] M. T. Bevacqua, R. Palmeri, T. Isernia, and L. Crocco, "Some considerations on the physical meaning of orthogonality sampling method," in *2018 IEEE International Symposium on Antennas and Propagation USNC/URSI National Radio Science Meeting*, 2018, pp. 705–706.

[10] ——, "Physical interpretation of the orthogonality sampling method," in *2018 2nd URSI Atlantic Radio Science Meeting (AT-RASC)*, 2018, pp. 1–3.

[11] M. N. Akıncı, M. Cayoren, and I. Akduman, "Near-field orthogonality sampling method for microwave imaging: Theory and experimental verification," *IEEE Transactions on Microwave Theory and Techniques*, vol. 64, no. 8, pp. 2489–2501, 2016.

[12] M. N. Akıncı, "Improving near-field orthogonality sampling method for qualitative microwave imaging," *IEEE Transactions on Antennas and Propagation*, vol. 66, no. 10, pp. 5475–5484, 2018.

[13] A. Cheraghi, "A study on using linear electromagnetic imaging methods for obtaining the grain/air interface inside metallic-walled grain storage bins." University of Manitoba, MSc. Thesis., 2022-04-28.

[14] A. Cheraghi, I. Jeffrey, and C. Gilmore, "Using lossy green's functions to improve back-propagated reconstructions of material interfaces inside resonant enclosures," in *2021 IEEE 19th International Symposium on Antenna Technology and Applied Electromagnetics (ANTEM)*. IEEE, 2021, pp. 1–2.

[15] A. Baran, J. LoVetri, D. Kurrant, and E. Fear, "Immersion medium independent microwave breast imaging," in *2017 XXXIInd General Assembly and Scientific Symposium of the International Union of Radio Science (URSI GASS)*. IEEE, 2017, pp. 1–4.

[16] P. M. Van Den Berg and R. E. Kleinman, "A contrast source inversion method," *Inverse problems*, vol. 13, no. 6, p. 1607, 1997.

[17] M. T. Bevacqua, T. Isernia, R. Palmeri, M. N. Akinci, and L. Crocco, "Physical insight unveils new imaging capabilities of orthogonality sampling method," *IEEE Transactions on Antennas and Propagation*, vol. 68, no. 5, pp. 4014–4021, 2020.

[18] R. Potthast, "A study on orthogonality sampling," *Inverse Problems*, vol. 26, no. 7, p. 074015, 2010.

[19] N. Abdollahi, I. Jeffrey, and J. LoVetri, "Non-iterative eigenfunction-based inversion (niei) algorithm for 2d helmholtz equation," *Progress in Electromagnetics Research B*, vol. 85, pp. 1–25, 2019.

[20] I. Jeffrey, A. Zakaria, and J. LoVetri, "Microwave imaging by mixed-order discontinuous galerkin contrast source inversion," in *2014 XXXIth URSI General Assembly and Scientific Symposium (URSI GASS)*. IEEE, 2014, pp. 1–4.

[21] C. Geuzaine and J.-F. Remacle, "Gmsh: A 3-d finite element mesh generator with built-in pre-and post-processing facilities," *International journal for numerical methods in engineering*, vol. 79, no. 11, pp. 1309–1331, 2009.

[22] P. Van den Berg and A. Abubakar, "Contrast source inversion method: State of art," *Progress in Electromagnetics Research*, vol. 34, pp. 189–218, 2001.